The YAK-AEROSIB transcontinental aircraft campaigns: new insights on the transport of CO_2, CO and O_3 across Siberia

By J.-D. PARIS[1]*, P. CIAIS[1], P. NÉDÉLEC[2], M. RAMONET[1], B. D. BELAN[3],
M. YU. ARSHINOV[3], G. S. GOLITSYN[4], I. GRANBERG[4], A. STOHL[5], G. CAYEZ[2],
G. ATHIER[2], F. BOUMARD[1] and J.-M. COUSIN[2], [1]*Laboratoire des Sciences du Climat et de
l'Environnement, IPSL, Orme des Merisiers, CEA-CNRS-UVSQ, 91190 Gif-sur-Yvette, France;* [2]*Laboratoire
d'Aérologie, CNRS-UPS, Toulouse, France;* [3]*Zuev Institute of Atmospheric Optics, SB-RAS, Tomsk, Russia;* [4]*Obukhov
Institute of Atmospheric Physics, RAS, Moscow, Russia;* [5]*Norwegian Institute for Air Research, Kjeller, Norway*

ABSTRACT

Two airborne campaigns were carried out to measure the tropospheric concentrations and variability of CO_2, CO and O_3 over Siberia. In order to quantify the influence of remote and regional natural and anthropogenic sources, we analysed a total of 52 vertical profiles of these species collected in April and September 2006, every ∼200 km and up to 7 km altitude. CO_2 and CO concentrations were high in April 2006 (respectively 385–390 ppm CO_2 and 160–200 ppb CO) compared to background values. CO concentrations up to 220 ppb were recorded above 3.5 km over eastern Siberia, with enhancements in 500–1000 m thick layers. The presence of CO enriched air masses resulted from a quick frontal uplift of a polluted air mass exposed to northern China anthropogenic emissions and to fire emissions in northern Mongolia. A dominant Asian origin for CO above 4 km (71.0%) contrasted with a dominant European origin below this altitude (70.9%) was deduced both from a transport model analysis, and from the contrasted $\Delta CO/\Delta CO_2$ ratio vertical distribution. In September 2006, a significant O_3 depletion (∼ −30 ppb) was repeatedly observed in the boundary layer, as diagnosed from virtual potential temperature profiles and CO_2 gradients, compared to the free troposphere aloft, suggestive of a strong O_3 deposition over Siberian forests.

1. Introduction

The purpose of the YAK-AEROSIB aircraft campaigns is to document the composition and the large-scale synoptic transport of CO_2, CO and O_3 into the Siberian air shed. The data resulting from two campaigns in April and September 2006 are presented.

CO_2 is the main anthropogenic greenhouse gas in the atmosphere. Also a significant greenhouse gas, tropospheric O_3 is a pollutant harmful to human and vegetation. O_3 and CO are important components of the atmospheric chemical system. Tropospheric O_3 sources are photochemical production from precursors such as CO and volatile organic compounds (VOCs), and stratospheric input. It is removed by ground deposition and photodissociation. The main net sources of CO_2 and CO are combustion processes. CO_2 sinks are terrestrial photosynthesis and oceanic uptake.

Siberia is a key region for the global carbon cycle with a CO_2 sink of 0.5 ± 0.5 GtC yr^{-1} (Gurney et al., 2002), but its magnitude is not constrained by any surface stations inside Siberia. In addition, Siberia is a region where atmospheric transport models fail to represent the vertical profiles of atmospheric CO_2, due to covariations between ecosystem fluxes and vertical transport on seasonal time scales (Gurney et al., 2002; Stephens et al., 2007). Both the transport and the surface fluxes of CO_2 over Siberia (e.g. van der Molen and Dolman, 2007) are poorly known.

The seasonal cycle of CO_2 over the Eurasian continent has only been measured at sparse locations by means of tall tower (e.g. Maksyutov et al., 2006), or occasional or monthly vertical profiles in the lower troposphere (Machida et al., 2001; Levin et al., 2002; Lloyd et al., 2002; Ramonet et al., 2002; Hiyama et al., 2003). Snapshot boundary layer (BL) budget studies were executed in Siberia (Lloyd et al., 2002; Ramonet et al., 2002) but the inference of sources and sinks from these data using 1-D models suffers from ignoring the true 3-D complexity of regional circulations (van der Molen and Dolman, 2007). The YAK-AEROSIB data bridge this gap of scales by taking dense

measurements across the entire Siberian air shed. Dense CO_2 vertical profiles are needed to better understand how ecosystem CO_2 fluxes are coupled to atmospheric transport.

In addition to large-scale transport of natural and anthropogenic fluxes, the variability of CO_2 over continents is also driven by synoptic frontal passages (Chan et al., 2004; Wang et al., 2007), mesoscale regional circulations and BL dynamics (Nakazawa et al., 1997; Nicholls et al., 2004; Sarrat et al., 2007; Wang et al., 2007). Dense vertical profiles and horizontal gradients of CO_2 over continents obtained with airborne campaigns provide unique insights to better quantify and understand the variability of the underlying CO_2 sources and sinks. For instance, Gerbig et al. (2003) and Lin et al. (2003) provided a new measure of the spatial coherence scale of CO_2 in the BL, showing that transport models should have a resolution of at least 30 km to capture it.

Like for CO_2, in addition to natural processes, the tropospheric composition over Siberia for CO and O_3 reflects also long-range transport (LRT) (e.g. Newell and Evans, 2000; Bey et al., 2001; Stohl, 2001; Eckhardt et al., 2004; Wild et al., 2004; Stohl et al., 2007a, b). Wild et al. (2004) found for instance a net ozone enhancement over Siberia due to European precursor emissions. Transport of pollutants across Eurasia, and into Siberia, have received little attention (Akimoto, 2003). Data from the Mondy station in the Baikal area (Pochanart et al., 2003), and from the TROICA train transects (Bergamaschi et al., 1998; Crutzen et al., 1998; Oberlander et al., 2002) have provided a ground-based view of the gradients and origin of CO and O_3 in Siberia. Pochanart et al. (2003) documented a spring maximum and summer minimum of both CO and O_3 concentrations. They found that the most enhanced concentration levels of CO and O_3 in Baikal Lake region were observed in

air masses transported from Europe. In the upper troposphere, high CO levels of 150 ppb (30% above the hemispheric background) caused by widespread forest fires have been measured over eastern Siberia during summer (Nédélec et al., 2005), indicating that fire emissions can be uplifted at high altitude over the region. Large gaps remain in understanding pollutant transport and chemistry across Eurasia.

The two YAK-AEROSIB campaigns presented here sampled the tropospheric concentrations of CO_2, CO, O_3 and of fine aerosols across a large horizontal transect between Novosibirsk (central Siberia) and Yakutsk (eastern Siberia) during 7–10 April and 11–14 September, 2006. We first describe the in-situ instrumentation for continuous measurements of CO_2, CO and O_3 (Section 2), the synoptic weather conditions during each campaign (Section 3), and the associated trace gas distribution (Section 4). In Section 5, the fast upwards transport of Chinese pollution through a frontal event in April 2006 is analysed. In Section 6, the correlation between CO and CO_2 variations in the profiles and their potential use to trace the fossil component of CO_2 is studied. Throughout this manuscript 'BL' refers to boundary layer and 'FT' to free troposphere.

2. Campaign and instrumentation description

2.1. Study area

The flight pattern of the YAK-AEROSIB campaigns is shown in Fig. 1. It covers the lowermost 7 km of the troposphere from 55°N to 63°N between 80°E and 130°E. The ground is mainly forested by coniferous trees and partly covered by agricultural regions further south and west (Bartalev et al., 2003). The northwestern quarter of the area lies in zones of continuous permafrost

Fig. 1. Campaign flight plan: general view and detailed 3D view with flight pattern designed to optimize vertical soundings. The actual flights shown are Flights 1 (green), 2 (red), 3 (blue) and 4 (black). Flights 5–8 follow similar routes, with plateaux at 5 km instead of 2 km. The squares labelled NOV and YAK indicate the cities of Novosibirsk and Yakutsk, respectively. MND, KZD and KZM indicate the stations of Mondy, Sary Taukum and Plateau Assy, respectively.
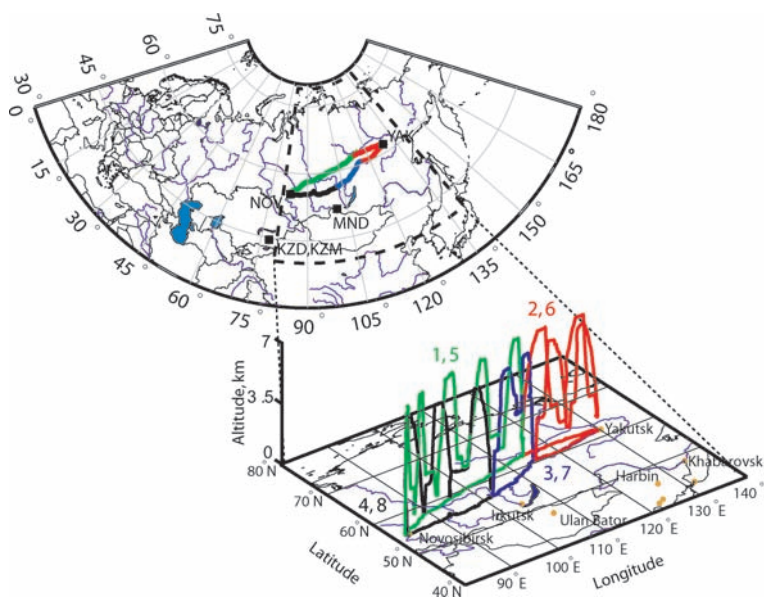
Table 1. Summary of flights during the YAK-AEROSIB campaigns in 2006

Flight nb	Day	Time (local)	Time (UTC)	Nb profiles	Itinerary
1	11 Apr 06	1200–2100	0600–1200	8	Novosibirsk-Myrni
2	12 Apr 06	1100–1530	0200–0630	8	Myrni-Yakutsk-Lensk
3	12 Apr 06	1730–1900	0830–1100	4	Lensk-Bratsk
4	14 Apr 06	0830–1030	0030–0430	6	Bratsk-Novosibirsk
5	07 Sept 06	0900–1900	0300–1000	10	Novosibirsk-Myrni
6	08 Sept 06	0945–1430	0045–0530	8	Myrni-Yakutsk-Lensk
7	08 Sept 06	1600–1730	0700–0930	2	Lensk-Bratsk
8	10 Sept 06	0900–1115	0100–0515	6	Bratsk-Novosibirsk

(100–500 m thick), and discontinuous permafrost in the South. The region has an extensive network of rivers and lakes, including the Yenissei and Lena rivers and their contributors. Forested bogs are also present near the track.

A number of cities are crossed: Novosibirsk, Tomsk, Mirny, Yenisseisk, Irkutsk, Bratsk, Krasnoyarsk and Kemerovo. Most of them are industrial or mining centres. The areas surrounding Krasnoyarsk and Novosibirsk are also covered by agriculture. Figure 1 shows the YAK-AEROSIB route with the starting point Novosibirsk (NOV) and the easternmost pivot point Yakutsk (YAK). Figure 1 also indicates the location of ground-based atmospheric mountain stations Mondy (MND; 51°39N, 100°55E, 2006 m a.s.l.) in Russia, near the Baikal Lake, and of Sary Taukum in Kazakhstan (KZD, 43°15N, 77°53E, 412 m a.s.l.) and Plateau Assy, Kazakhstan (KZM, 43°13N 77°53E, 2519 m a.s.l.) which are part of the global ESRL air sampling network. Other stations of interest for this study are Barrow in Alaska (BRW), 71°19N, 156°36E, 11 m a.s.l.) and Pallas in Northern Finland (PAL, 67°58N, 24°07E, 560 m a.s.l.). Data from these stations are compared to the aircraft profiles in Section 4.

2.2. *Campaigns description*

The two YAK-AEROSIB campaigns followed the same route. Each campaign consists of four flights shown with different colours in Fig. 1. The YAK-1 campaign was conducted in April 2006. A series of 26 vertical profiles were collected. Each profile takes about 30 min, including horizontal plateaus at 0.5 and 7 km, and at 5 km on descents. The YAK-2 campaign was conducted in September 2006 and included 26 vertical profiles, with plateaus at 0.5 and 7 km, and 2 km on descents (see Table 1 for a summary). The chartered aircraft is a two-propeller Antonov-30 (see Fig. 2 for a picture of the aircraft and a representation of the inside instrumental setup) operated by the Institute of
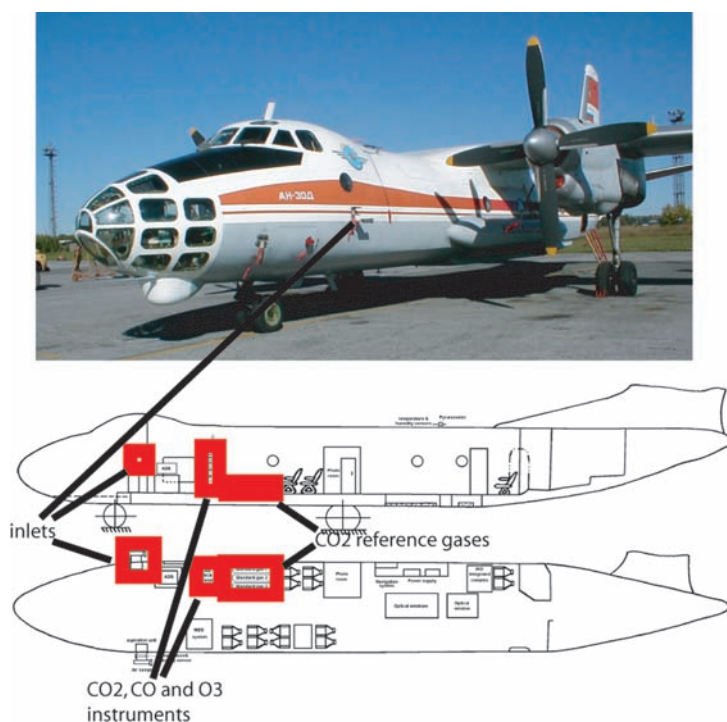

Fig. 2. The Antonov-30 'Optik-E' aircraft operated by IAO. (a) picture from outside, inlet are signalled by red tissues and (b) schematics of the interior of the aircraft. The instruments giving the data studied in this paper are highlighted in red.

Atmospheric Optics of Tomsk (Zuev et al., 1992). The maximum range of the aircraft is 3400 km and its airspeed during measurement is about 85 m s^{-1}. Vertical speed during vertical profiles is about 3.5 m s^{-1} on ascent and 7 m s^{-1} on descent.

The flights were performed in all-weather conditions. During Flight 1 (11 April 2006) at 1030 UTC and in Flight 7 (8 September 2006) at 0800 UTC the profiles have not been completed down to the ground because of excessive cloudiness. The times of flights were dependent on logistical constraints. The April flights were carried mostly in the local afternoon, whereas the September flights started at 0900 LT (Table 1). The long duration of the flights allowed sampling a large diversity of combinations of air masses, cloudiness conditions, solar zenith angles and vegetation cover types. Diurnal variations of the BL height are expected to affect the comparability of individual profiles, but these differences tend to compensate over a whole flight, when making composite profiles. Synoptic variations are discussed in latter sections. In April, the sunrise occurs at about 0530 LT-Novossibirsk (GMT + 0600), and sunset at 1945 LT-Novossibirsk, that is, a photoperiod length of 14.3 h. In September, the sunrise was at 0550 LT and sunset at 1930, that is, a photoperiod of 13.7 h.

2.3. Onboard instruments

2.3.1. CO$_2$. The CO$_2$ analyser is a Li-Cor 6262 modified non-dispersive infrared (NDIR) analyser modified at the LSCE. The Li-Cor is embedded in a system which regulates the temperature, flow and pressure of incoming air. Sampled air is dried upstream using magnesium perchlorate. Pressure fluctuations within 0.5 mbar around target value pressure are allowed in the data processing. Acquisition frequency is 0.5 Hz. In-flight calibrations are performed at 30 min intervals using three calibration gases. These gases are carried in high-pressure cylinders that are used sequentially ('high', 'low' and 'reference' value). Their values were determined at the LSCE laboratory prior to shipment and are traceable to a suite of primary WMO-CO$_2$ standards from NOAA/ESRL. The concentrations used are 370.60 ± 0.01, 380.47 ± 0.01 and 409.76 ± 0.01 ppm, respectively. The three calibration gases are analysed during the flight at ∼30 min intervals. The drift is corrected for based on errors in estimation of reference gas. During the April 2006 campaign, the precision was 0.4 ppm and accuracy 0.15 ppm. Improvements in the electronics yielded a precision of 0.15 ppm for the September 2006 campaign. The CO$_2$ instrument precision is estimated from the standard deviation of the stabilized concentration signal during 1 min after injecting the reference gas, allowing 2 min for stabilization in the measurement cell. The accuracy is estimated as the offset of the instrument when measuring a 'target' reference gas cylinder during 1-min in the pressure-stabilized cell. The CO$_2$ data are processed using a semi-automatic filter based on pressure, flow and temperature in the measurement and reference cells of the Li-Cor.

2.3.2. O$_3$. The O$_3$ analyser is developed from a commercial fast response ozone analyser (Thermo Instruments Model 49), with modifications for internal calibration and aircraft operation safety. The instrument is based on classic UV absorption in two parallel cells (zero, sample), with a precision of 2 ppb, 2% for an integration time of 4 s. It is compensated for aircraft pressure and temperature variations. Prior to detection, air is pressurized to cabin pressure, using a Teflon KNF Neuberger pump model N735 also used for the CO instrument. Electrical improvements has been brought by Laboratoire d'Aérologie, including a 27VDC supplied power provided also to the CO instrument. For the YAK-AEROSIB project, the ozone instrument includes a specially designed computer for data acquisition and for instrument control, powered in aircraft 27VDC. Before shipping to Russia, the O$_3$ analyser has been calibrated against a NIST related reference calibrator Model49PS. A calibration box with an O$_3$ generator is used for laboratory verifications of the ozone analyser before and after the campaigns.

2.3.3. CO. The CO analyser has been described in Nédélec et al. (2003). It is a fully automated instrument designed to reach an accuracy of 5 ppb or 5%. The instrument is based on a commercial infrared absorption correlation gas analyser (Model 48C, TEI Thermo Environment Instruments, USA). The model 48CTL is qualified by U.S. EPA designated method EQSA-0486–060. Laboratoire d'Aérologie improved the instrument accuracy with addition of periodical (every 20 min), in-flight accurate zero measurements, new IR detector with better cooling and temperature regulation, pressure increase and regulation in the absorption cell, increased flow rate to 4 l min^{-1}, water vapour trap and ozone filter. The precision achieved for 30 s integration time (corresponding to the response time of the instrument) is 5 ppb or 5% CO, with a lower detection limit of 10 ppb.

2.3.4. Meteorological parameters. Temperature, humidity and wind vector are measured routinely onboard using HYCAL sensor model IH-3602-C of Honeywell Inc. Temperature range is from −70 to +70°C and accuracy is 0.5°C. Relative humidity range is from 0 to 100% and accuracy is 7%.

3. Synoptic situation and transport

3.1. Lagrangian particle transport model

Atmospheric transport was investigated using FLEXPART (Seibert and Frank, 2004; Stohl et al., 2005). The model was run backward in time from small boxes (0.5° × 0.5° × 100 m) arranged along the flight tracks. The backward simulation method can be used to analyse air mass transport, relating potential source regions to the aircraft position. Each simulation consists of 20 000 particles released in the volume of air sampled, which were followed 20 d backward in time. The Potential Emission Sensitivity (PES) function is defined as the residence time of the backward particles in each particular grid box below

a given threshold altitude. The PES is a measure for the simulated mixing ratio at the receptor that a source of unit strength in the respective air column below the threshold altitude would produce, disregarding loss processes (passive tracer case). Two different FLEXPART setups are used to calculate PES in this paper: (1) the runs presented for analysing transport patterns (Sections 3.2 and 3.3 below) are done 10 d backward with PES up to 3000 m and (2) the run for the case study of north-eastern Asian emission uplift contributions (Section 5.1.) is done 20 d backward with PES up to 300 m.

3.2. Synoptic situation during April 2006 campaign

There were fair weather conditions during most of the campaign with occasional fair weather cumulus. The weather was, however, cloudy during Flight 1 (1000–1200 UTC) and precipitations occurred during Flight 4. The BL was shallow and stable during most of the campaign, due to cold near-ground temperature (between –5 and –15°C). During Flight 2 a strong temperature inversion was observed at ≈2 km altitude.

Figure 3a shows the ECMWF geopotential height at 500 hPa for 12 April 2006. Figures 3b–d shows the FLEXPART PES functions (<3000 m) up to 10 d backwards. The PES are summed for all the receptor locations corresponding to the aircraft route each day (panel 3c sums Flights 2 and 3). Red squares correspond to space borne fire detection from ATSR World Fire Atlas fire maps for periods 5–12 April (Figs. 3b–d) and 1–7 September (Figs. 3f–h), retrieved from http://dup.esrin.esa.int/ionia/wfa/. Stationary fires occur in North-western Siberia near 65°N, 80°E, associated to industrial gas flaring in the Norilsk region. Just before the April campaign, two local geopotential minima, over northern and eastern Siberia, cause advection of polar air in the Siberian troposphere. This is confirmed by the PES of Flights 1–3 (Figs. 3b and c), showing that the aircraft sampled mainly polar air below 3 km. Across Southern Siberia, a westerly flow is associated to a low pressure system centred at 65°N, 120°E (Fig. 3a). Between 11 and 13 April, stagnant conditions at 500 hPa lead to very slow stirring, or filamentation, of FT air. Under these stagnant conditions, there is no advection of European emissions and the footprint (Figs. 3b and c) remains concentrated over Siberia. During 11–12 April (Flights 1–3, Figs. 3b and c), advection in the lowermost troposphere towards the aircraft route occurs mostly from central Siberia.

Figure 4a shows the synoptic weather chart for 11 April 2006, at 0600 UTC. Prior to and during Flights 2–3, a series of fronts passed over northeastern Asia during four consecutive days. These fronts caused uplift of BL air from northeastern Asia. The combination of (1) stagnation in the middle FT and (2) uplift by the frontal passages of moist and warm air from Northern China and eastern Mongolia (see PES in Fig. 3c) resulted into the presence of a polluted air mass in the FT which was sampled by the aircraft (Section 5.1). For Flight 4 the situation is different, and the main PES, in addition to local Siberian sources, is found to occur just east of the Ural Mountains and in Central and Eastern Europe. According to ATSR fire maps, our measurements are sensitive to agricultural fires in Kazakhstan and to gas flaring emissions in the Norilsk area.

3.3. Synoptic situation during September 2006 campaign

The September campaign experienced mixed, variable weather. Fair weather occurred only during Flight 5, except at 0545 UTC, were a cloud formation was crossed (warm front). There were precipitations at the end of Flight 6 and beginning of Flight 7 with cold near-ground temperature, and intense convection afterward (Flight 7 at 0800 UTC). The end of Flight 8 also crossed convective conditions.

Figure 3e shows the ECMWF geopotential height at 500 hPa on 7 September 2006. Figures 3f–h show the FLEXPART PES (<3000 m) up to 10 d backwards reaching the aircraft locations. Figure 3g show the cumulated PES summed for the route of Flights 6 and 7. The period is characterized by a typical 'omega circulation' whirling around troughs over Eastern Europe and Eastern Asia. A ridge is located over central Siberia, associated with weak fronts (Fig. 4b). The European outflow is partially channelled towards (1) Turkey and the Black Sea by a low-pressure system in European Russia (Fig. 3e, at 60°N-45°E) and (2) central Siberia by a ridge moving eastward (over Kazakhstan at 50°N–70°E on 7 September). The polar low causes a fast northwesterly flow over central Siberia. The combination of zonal 'Omega' circulation and baroclinic perturbations in European Russia mixed up European emissions into the FT over Siberia at the time of the campaign. In addition to this influence from Europe, a significant part of the PES for this campaign (Figs. 3f–h) is located over Siberia and Kazakhstan, in presence of regional perturbations leading to local uplift of BL air.

Figure 4b shows the synoptic weather chart for 7 September 2006, at 1200 UTC (Flight 5). The dominant synoptic feature of the campaign is a warm front moving towards the South East on 7–8 September. The corresponding FLEXPART simulations of PES across both sides of the warm front indicate sharply distinct origins for the sampled air masses (not shown). For aircraft altitudes below the warm frontal surface (<1.5 km), the air has a polar origin, and spent at least 15 d into the Arctic. In contrast, for aircraft altitudes above the warm frontal surface (1.5–5 km), the air has a western origin and is sensitive to fire emissions in the Caspian Sea area (Figs. 3f and g). For altitudes greater than 5 km, the air has a remote origin, and has been entrained by a jet. The consequences on the measured CO_2 and CO profiles are discussed in Sections 4.1.1 and 4.1.2.

Figure 5 shows example vertical profiles of meteorological variables for 7 September 2006 (Flight 5), and the BL height diurnal variation deduced from these data. Figures 5a and b show the vertical profiles of temperature, wind vector, potential virtual temperature, relative humidity and water vapour mixing ratio
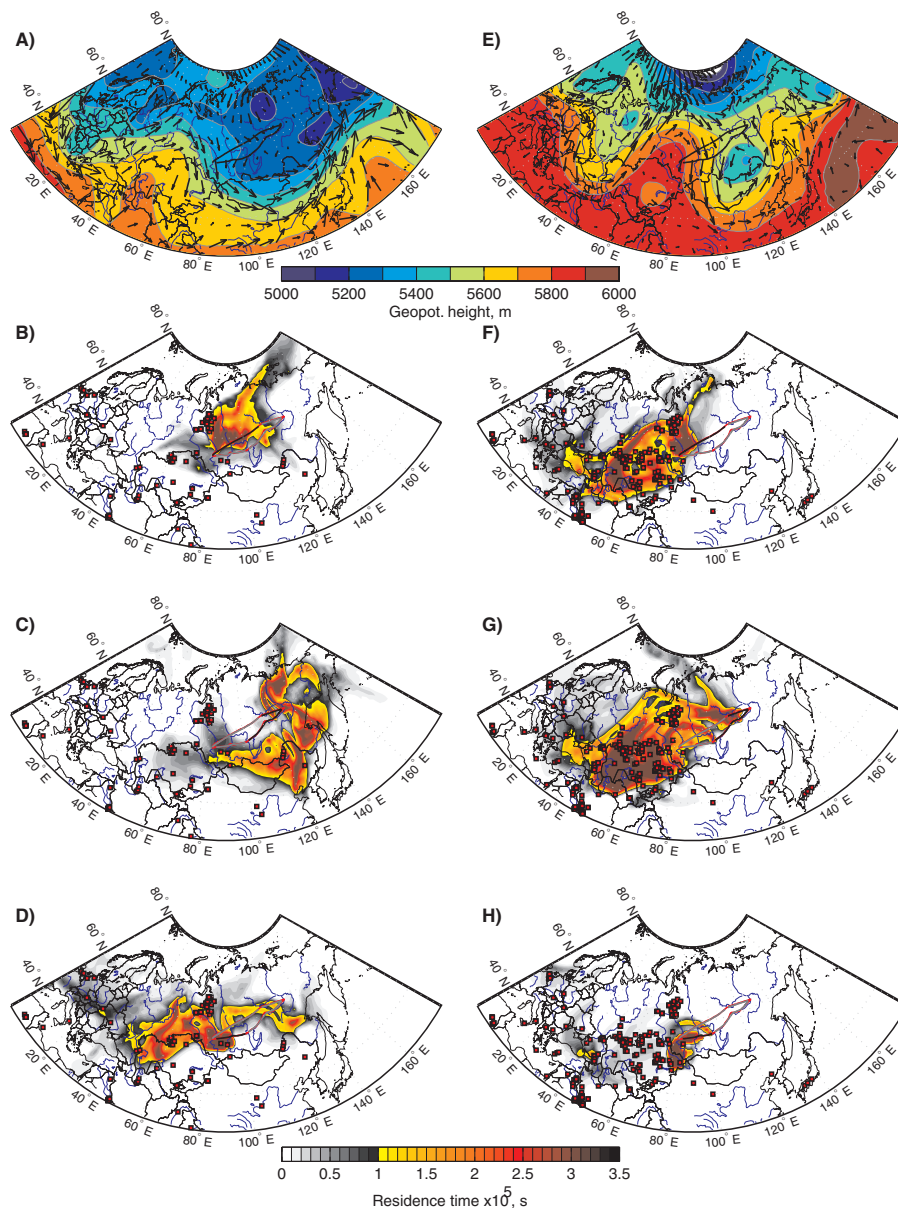
Fig. 3. Atmospheric transport patterns at the time of the campaigns. (a) Geopotential height and wind at 500 hPa from ECMWF analyses for 12 April at 0600 UTC. (b) 10-d potential emission sensitivity (PES) for simulated retro-transport of particles released along Flight 1, (c) same for Flights 2 and 3, and (d) for Flight 4. (e) same as (a) for 7 September at 0600 UTC, (f) PES for Flight 5, (g) for Flights 6 and 7 h) for Flight 8. Red squares represent ATSR World Fire Atlas for 5–12 April (b–d) and 1–7 September (f–h).

(WMR), during the two first ascents of Flight 5. The BL height in Fig. 5c is determined from consecutive profiles of virtual potential temperature, humidity and CO_2. On average across the flights, the mid-day average BL height during the September 2006 campaign was ≈1.2 km, and occasionally convective.

4. Tracers variability

Figures 6 and 7 show selected individual profiles for flights of the April and September campaigns. Time series from each campaign are further shown in Supplementary material on-line (Figs. S1 and S2). Figure 8 shows the average vertical profile of each flight, calculated for altitude bins of 1 km. Horizontal error bars represents the 10th and 90th percentiles of each bin. Monthly smoothed CO_2 and CO concentrations recorded at coincident times are shown for stations KZM (letter K), KZD (letter D), BRW (letter B) and PAL (letter P). The smoothed data were obtained from the NOAA ESRL website (http://www.esrl.noaa.gov/gmd/ccgg/iadv/, see stations location in Fig. 1). The spring and fall O_3 seasonal concentrations for
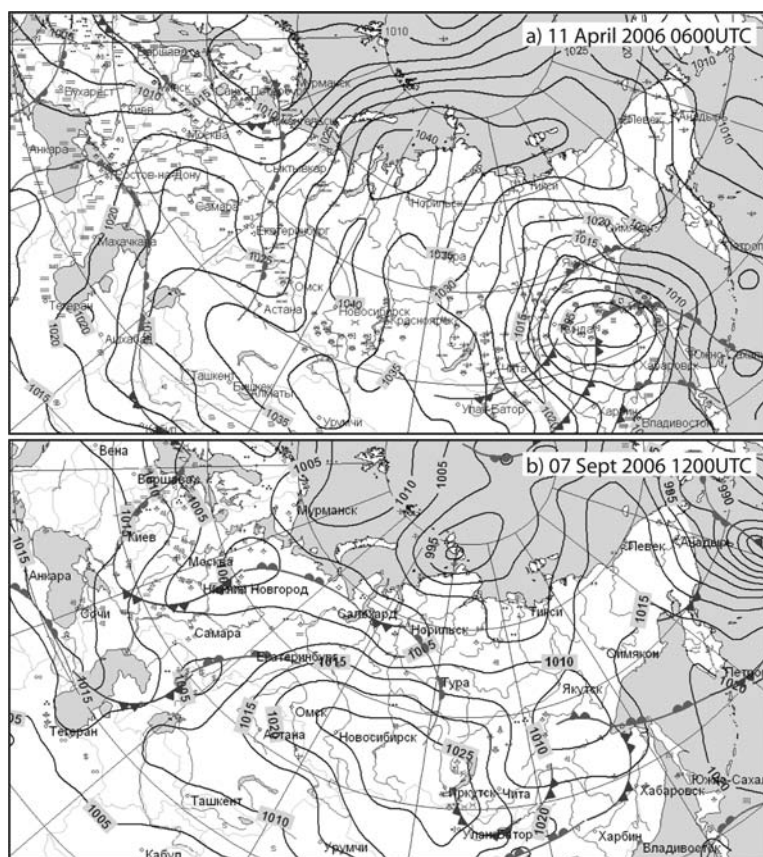
Fig. 4. Russian weather service Hydrometcenter charts. (a) 11 April 2006 at 0600 UTC. A series of fronts associated with a depression are moving south-eastward on the Eastern Asia coast. (b) 7 September 2006 at 1200 UTC. A warm front stretching between Norilsk and Krasnoyarsk was crossed by the YAK-AEROSIB aircraft during Flight 5.

the period 1997–1999 from Pochanart et al. (2003) are shown in Figs. 8c and f at the MND (letter M) mountain station, near the Baikal lake.

4.1. April 2006 campaign

4.1.1. CO₂ concentrations. An estimate of the background CO_2 concentration was calculated from the data, based on CO variability criteria. We binned the CO_2 data into 2 min intervals, rejected the bins where the *SD* of CO exceeded 10 ppb, took the 33rd percentile of CO_2 in each selected bin, and finally averaged all these values to define the background CO_2 of the campaign. This selection of low variability CO episodes is capable of efficiently discarding CO_2 in polluted layers. The April CO_2 background is 386.2 ± 1.7 ppm (grey line and shaded area in Fig. 8a), very close to the monthly smoothed KZM data (385 ppm in Fig. 8a). Note that the corresponding background CO for the campaign also agrees well with the KZM data (see below). The CO_2 and CO excesses above the background therefore reflect regional variability of transport. Elevated CO_2 concentrations near the surface, up to 393 ppm, were observed above Novosibirsk and Tomsk (Fig. 6i, Flight 4), or in layers separated from, but close to the surface (see e.g. Fig. 6e, near the city of Lensk at 1.5 km altitude). The coincident high concentrations of CO confirm that these elevated CO_2 values reflect the city

plumes where regional anthropogenic emissions accumulate in April below stable inversion layers.

4.1.2. High CO concentrations. The mean CO concentration measured during the April 2006 campaign is 174 ± 28 ppb, whereas the background concentration (defined on the same basis as above) is 135 ± 21 ppb (grey line and shaded area in Fig. 8b). The background CO is reasonably close to the 139 ppb value recorded in altitude at KZM, like for CO_2 (Figs. 8a and b). The YAK background CO is however lower than the values recorded at the surface at BRW and KZD stations by 27 and 20 ppb, respectively. The mean CO concentration is 9 ppb higher than the MND 1997–1999 spring average value (Pochanart et al., 2003). The median CO concentration below 1 km of altitude during Flight 1 and 2 are very close to the PAL concentration of about 172 ppb (Fig. 8). However, the footprint pattern in Figs. 8b and c suggests that, if advection of air from Northern Europe is the source of this similarity, the contact with pollutant emissions must have occurred earlier than 10 d before. Using the MOZAIC passenger aircraft data, Nédélec et al. (2005) found an April median value of 125 ppb in the upper troposphere (8– 10 km altitude). Below 1.5 km, the CO profiles show a high variability, ranging from near-background values over the forests (Fig. 6f, below 4 km) up to CO > 300 ppb in city plumes (Fig. 6i Flight 4 near Novosibirsk). Between 1.5 and 4 km, the CO vertical distribution is more homogeneous. On the whole,
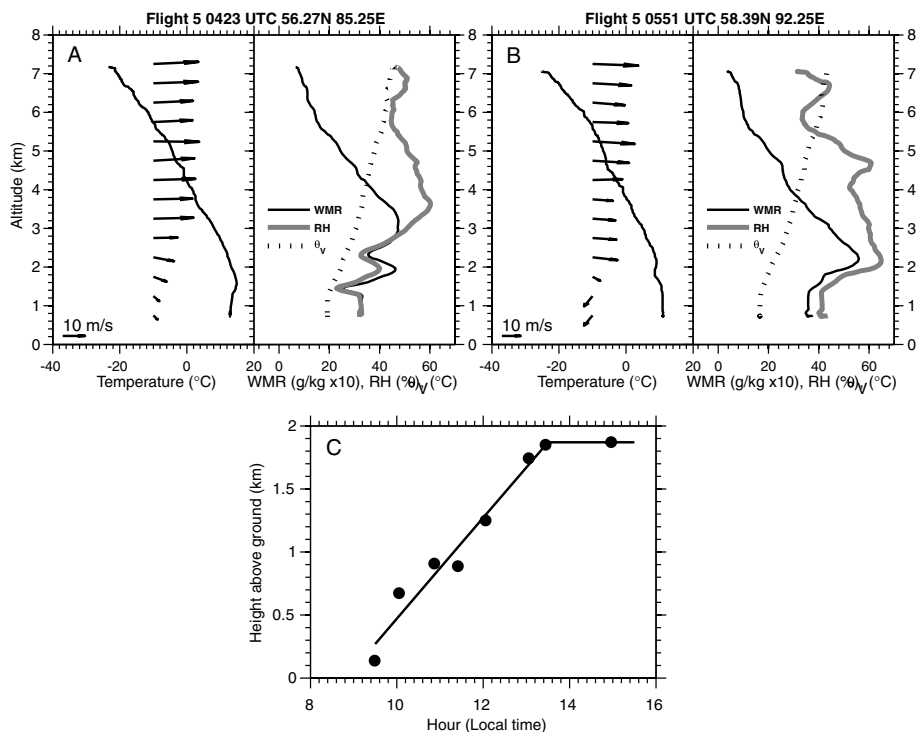
Fig. 5. Meteorological soundings of Flight 5. (A) vertical profile of (left-hand side) temperature and wind vector and (right-hand side) water vapour mixing ratio, relative humidity and virtual potential temperature during the ascent starting at 0423UTC. (B) Same as A for the ascent starting at 0551 UTC. (C) Boundary layer height above ground level deduced from virtual potential temperature, humidity and CO_2 profiles during Flight 5. Only BL heights with unambiguous profiles are included.

CO_2 and CO are highly correlated during the April 2006 campaign (see Fig. 9a). This is further analysed in Section 5.2.

4.1.3. O_3 concentrations. The O_3 concentration distribution measured in April 2006 is vertically fairly homogeneous in the FT, in the range of 50–60 ppb, although a well-defined increase of O_3 with height of 3 ppb km^{-1} can be observed between 1 and 6 km (Fig. 8c). The mean O_3 concentration measured during the entire campaign is 50 ± 5 ppb (Fig. 8c). The homogeneous O_3 distribution suggests no strong spatial gradients in chemical sources or sinks of O_3 affecting our profiles. 10–40 ppb depletion in O_3 is observed near the surface below 1 km, as compared to the FT above. The lowest O_3 near-ground minima are found over landing air-strips in polluted city plumes, which are easy to identify because of their elevated CO concentrations. This suggests a strong titration of O_3 by NO (Fig. 6i) near the surface. Note however that the anti-correlation between CO and O_3 is not systematic in high CO air masses.

During Flight 1, higher (>80 ppb) O_3 values above 6.5 km are observed. Highest O_3 concentrations range between 101 and 107 ppb and coincides with relatively low CO (126 ± 6 ppb) and low CO_2 values (385.0 ± 0.3 ppm) at 6.4 km altitude (Fig. 6a). This suggests a stratospheric contribution to the O_3 enhancement.

The mean O_3 concentration matches well the MND monitoring station spring value (Fig. 8c; Pochanart et al., 2003).

This good match also suggests that there is little year-to-year variability in springtime tropospheric O_3 concentration over Siberia.

4.1.4. Free tropospheric CO_2 and CO layer structure. Filaments with elevated CO_2 concentrations (4–6 ppm enhancement above background) and CO (60 ppb enhancement) were encountered at all altitudes, especially during Flight 2 and 3 (Figs. 6c–f). Associated CO values reach up to 250 ppb. The typical thickness of the layers is between 200 and 2000 m. The vertical profiles (e.g. Figs. 6d and e) suggest that the layered structure extends above the flight ceiling. This distribution of CO_2, also clearly visible in CO data, is due to slow stirring in the troposphere under reduced vertical mixing (Newell et al., 1999; Stohl, 2001; see CO–CO_2 scatter plots in Figs. 9a–d). Both the number of layer occurrence and their CO_2 excess above the background are higher in Flights 2 and 3 (which correspond to the easternmost part of the campaign flight track), than in Flight 1 and 4 over southwestern Siberia (see also Figs. 8a and b). O_3 shows no clear enhancement or depression in these layers. The reasons of this distribution will be examined in Section 5.1.

4.2. September 2006 campaign

4.2.1. CO_2 concentrations. In the September 2006 campaign, the background CO_2 concentration is 377.1 ± 0.9 ppm (same

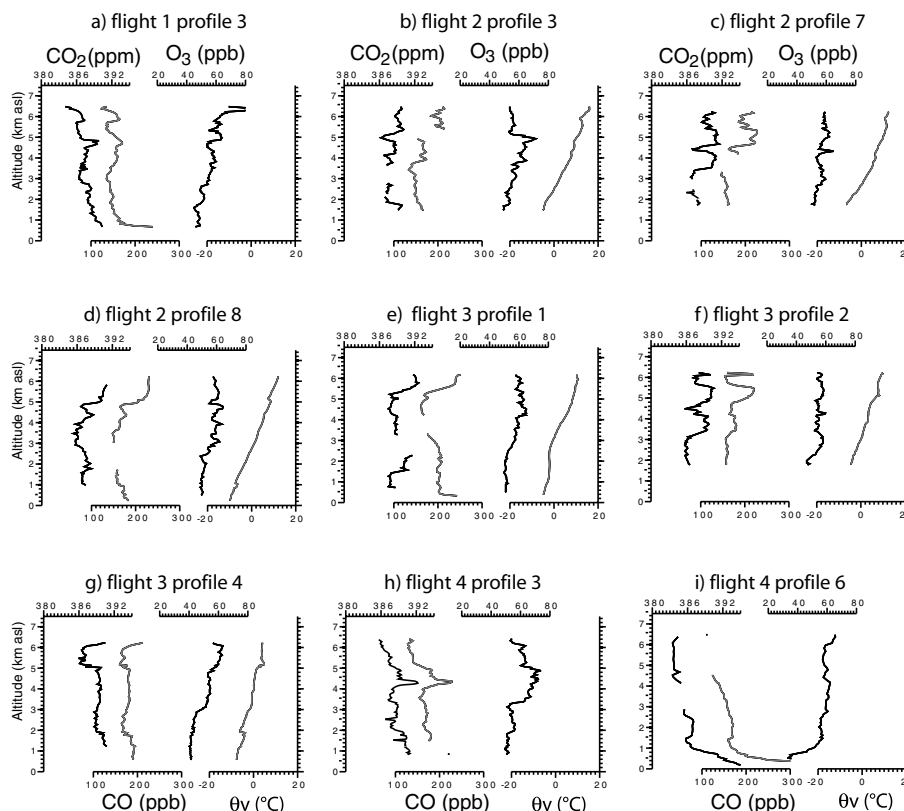*Fig. 6.* Nine selected vertical profiles of the April 2006 campaign which are discussed in the text. The CO_2 profiles are in thick black to the left-hand side of each plot, CO in light grey, O_3 in black and potential temperature in dark grey to the right-hand side of each plot.

method as April, see Section 4.1.1) which is 9 ppm less than in April 2006. The September 2006 CO_2 concentrations show no thin, stratified structure as in April, but plumes are observed in CO data. However, the meteorological conditions and the complex PES footprints shown by Figs. 3f–h suggest the contribution of air masses with distinct origins to the vertical profiles. From an analysis of the FLEXPART results, we inferred mostly an Arctic/boreal origin for CO_2 anomalies in the BL, and influence from more remote western sources (Kazakhstan) for CO_2 in the FT.

All the September individual CO_2 profiles (Figs. 7 and 8d) are characterized by decreasing values towards the surface. On Flights 5 and 7, CO_2 in the BL is depleted by an average of 4 ppm compared to the FT above (Fig. 8d). The BL CO_2 values during the entire campaign are on average 8 ppm lower than the ground based KZD station data (∼378 ppm) and 5 ppm lower than the BRW station data. The mean vertical September CO_2 gradient between KZM (2519 m a.s.l.) and KZD (412 m a.s.l.) is only ≈0.5 ppm, whereas in our data the Flight 5 CO_2 gradient at equivalent altitudes is 2–5 ppm (Fig. 8d). The FLEXPART analysis (Section 3.3 and Fig. 3b) shows that the air mass origin of the lowermost 1.5 km section of Flight 5 (BL) is from the Arctic, with a slow southward motion of air and lack of entrainment across the top of the BL. BRW is representative of mean Arctic

air concentration. The September campaign background CO_2 value is also very close to the BRW data (374.9 ppm). Therefore the 5 ppm CO_2 gradient between YAK concentrations in the BL (Flight 5) and BRW must be caused by regional biospheric uptake. FLEXPART backward transport analysis suggests that, in addition to regional differences in ecosystems uptake, associated with cropland and grasslands in Southern Siberia and Kazakhstan, regional variations in transport patterns between YAK (Flight 5) and KZD could contribute significantly to the gradient between these two locations.

Vertical profiles regularly collected at Zotino (65°45N, 89°23E; Lloyd et al., 2002) show that the mean BL-FT gradient at Zotino is slightly positive in September (1.39 ppm). The local afternoon BL height in September (Lloyd et al. 2002) is on average lower (0.7–1 km) than that observed during our campaign. The variability of CO_2 in the FT reflects advection of fossil fuel and biomass burning CO_2 (see Figs. 3f–h, red squares), regional differences in uptake by ecosystems, and stratospheric air influence. During Flight 5, both profile 2 (Fig. 7b) and profile 8 (Fig. 7e) at ∼6 km altitude show a coincident excess in O_3 and deficit in CO. In profile 2, the O_3 excess is 12 ppb and the CO deficit is 20 ppb (respectively 8 and 30 ppb in profile 8). Excess is defined here as the difference with the lower part of each profiles. This signature is consistent with a stratospheric
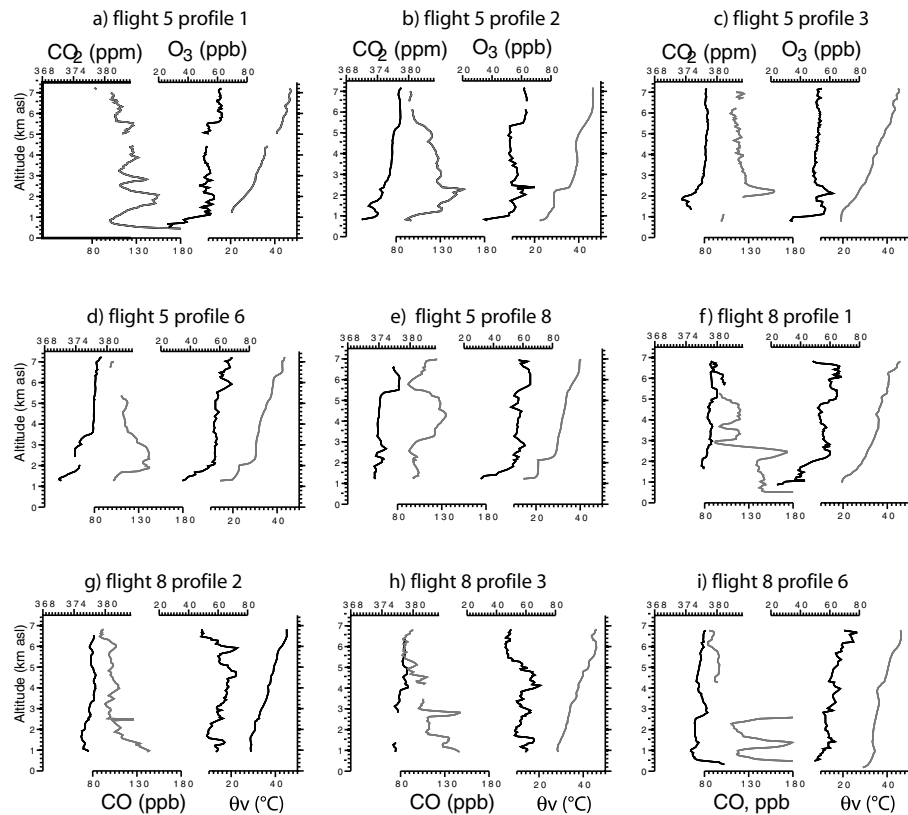
Fig. 7. Same as Figure 6 but for the September 2006 campaign.

Fig. 8. CO$_2$, CO and O$_3$ average
concentration profiles, for each flight. (a)
April 2006 CO$_2$ profiles for Flights 1–4. The
campaign background mean value and the
associated 1σ uncertainty are indicated by
the dark grey line and the light grey surface,
respectively. (b) Same as (a), for April 2006
CO profiles. (c) April 2006 O$_3$ profiles. (d)
September 2006 CO$_2$ profiles and
background for Flights 5–8. (e) September
2006 CO profiles. (f) September 2006 O$_3$
profiles. The horizontal error bars indicate
the 10th and 90th percentiles. Also shown
are the NOAA ESRL network interpolation
of measured CO$_2$ and CO at 10 April 2006
(a and b) and 15 September 2006 (d and e),
represented by a letter for KZM (K), KZD
(D), PAL (P) and BRW (B). O$_3$ is compared
with 3 year seasonal average at MND (M)
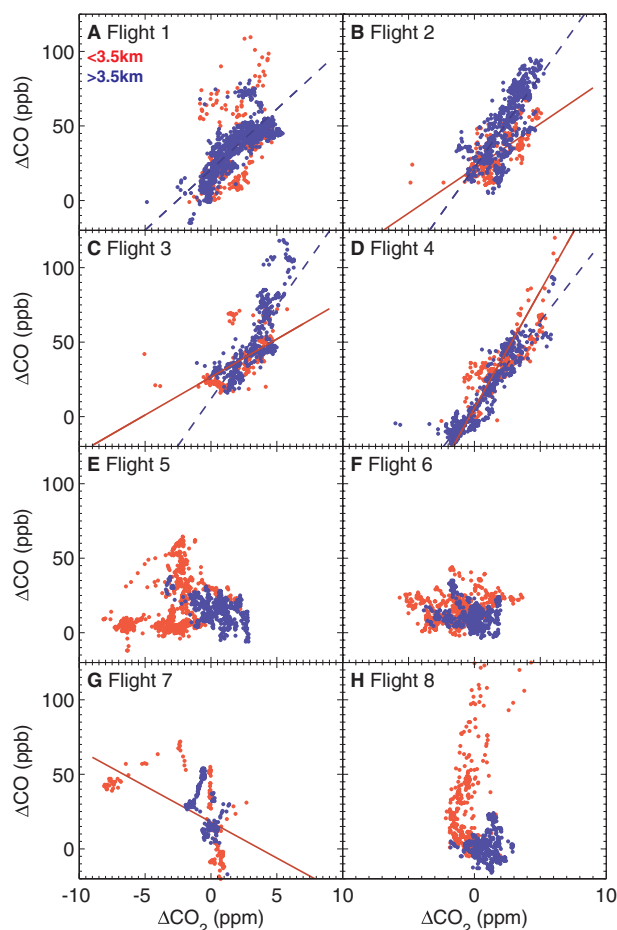for spring and fall.
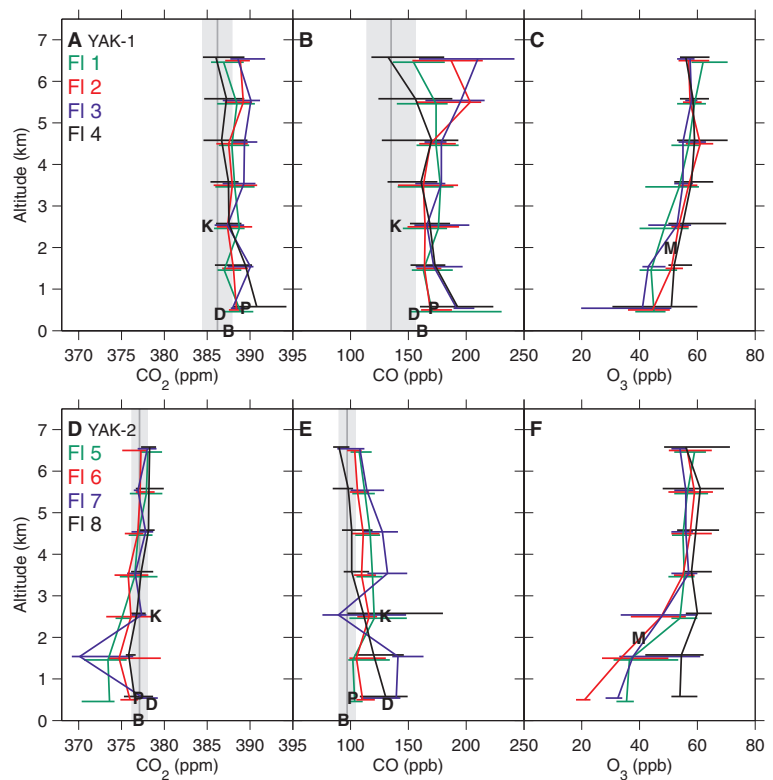
Fig. 9. Scatter plots of CO vs. CO_2 for all April and September flights. Red dots are for data below 3.5 km, blue dots are above 3.5 km. Regression slopes above (dashed blue line) and below 3.5 km (red line) are shown when correlation coefficient $R^2 > 0.25$. (a–d) Flights 1–4 in April 2006. (e–h) Flights 5–8 in September 2006. Note the absence of correlation for the September flights.

influence. Profile 2 and profile 8 (Figs. 7b and e) also show a positive excess of CO_2 (respectively 1 and 4 ppm) indicating that at this time of the year (end of the growing season), the mean lower stratospheric CO_2 is higher than the tropospheric CO_2 value depleted by net plant uptake.

4.2.2. CO concentrations. The CO background value for the September 2006 campaign is 97 ± 7 ppb (to be compared to 135 ± 21 ppb in April). This background CO is 30 ppb lower than measured further south at KZD and KZM, which may be more influenced by biomass burning (see fire counts in Fig. 3). The YAK CO background is comparable however to the value recorded further north at PAL and BRW stations (Fig. 8e).

The CO mean and standard deviation are 113 ± 30 ppb. In contrast to April, the air masses that were sampled in September were mostly influenced by surface fluxes from Siberia and Europe entrained by zonal 'Omega' advection (see PES in

Fig. 3). More active photochemical sink of CO oxidation contributes to decrease the CO September background concentration.

In the September profiles, plumes with CO enhancements up to 140–150 ppb were observed in the FT (mainly during Flight 5, at approximately 2 km altitude in Figs. 7a–c). As discussed in section 3.3, this is due to remote fires in Kazakhstan area and anthropogenic emissions advected in a warm air mass. These plumes also exhibit marked O_3 enhancements (Figs. 7b and c, at 2.5 km altitude). These CO September enhancements are much lower than in April.

4.2.3. Comparison of CO data with MOZAIC flights. Both in April and September, our CO average profiles in Siberia are higher than the European average concentration profiles, and lower than East Asian profiles, showing pollutant enrichment along the zonal flow. In the MOZAIC passenger aircraft CO climatology (http://mozaic.aero.obs-mip.fr), the CO profiles over Frankfurt (Germany) are in the range 130–140 ppb in April and 100–110 ppb in September. The MOZAIC CO concentrations are found to be higher over Nagoya, Osaka and Tokyo (Japan), with values of 140–180 ppb in April, and 120–130 ppb in September. The MOZAIC CO range between Germany and Japan brackets the values observed for each YAK-AEROSIB campaign. However, the CO profiles over Japan are influenced by Southern Asian sources, and not by the result of simple zonal advection of integrated northern Eurasian fluxes.

4.2.4. CO-CO_2 correlations. The scatter plots of ΔCO vs. ΔCO_2 for each flight of the September 2006 campaign are shown in Figs. 9e–h. Near the surface, we observe a CO concentration increase (Figs. 7a, f, h and i,) over cities, especially during Flight 8 over Bratsk and Novosibirsk (Figs. 7f, h and i). However in the presence of biospheric CO_2 uptake and photochemical activity, CO has no correlation with CO_2 in these city plumes in September. For comparison, in April we observed $R^2 = 0.95$ and 0.82, in the Novosibirsk and Tomsk plumes (see Flights 4 and 1). In September, the overall correlation between ΔCO and ΔCO_2 is small. This is seen in Table 2 and Figs. 9e–h. Comparing altitudes below 3.5 km, which are more influenced by regional fluxes, the correlation is much lower in September (R^2 range = 0.10–0.30) than in April (range = 0.24–0.60; Table 2). This shows the influence of biogenic sinks (no CO-CO_2 correlation in fluxes) superimposed with the one of anthropogenic emissions. In addition, during spring and summer, CO has additional sources and sinks (production from BVOC, and OH reaction) which de-correlate ΔCO and ΔCO_2 in the atmosphere (Turnbull et al. 2006). Rivier et al. (2006) also showed, using a model, that the CO to fossil fuel CO_2 regression slopes also have a maximum noise in summer.

4.2.5. O_3 concentrations and possible contributions. Beekman et al. (1994) have shown that free tropospheric O_3 concentrations in the northern hemisphere peaks in spring with a secondary maximum in summer. In our data the September O_3 tropospheric concentrations were slightly higher (55–65 ppb)

Table 2.   Summary of CO–CO$_2$ correlation by flight and by altitude

Flight	All altitudes		$z > 3.5$ km		$z < 3.5$ km	
	N	R^2	N	R^2	N	R^2
1	1315	0.44	939	0.59	376	0.24
2	858	0.53	646	0.59	212	0.50
3	553	0.54	371	0.65	182	0.35
4	711	0.74	484	0.87	227	0.60
5	1251	0.00	557	0.25	694	0.09
6	994	0.00	486	0.05	508	0.09
7	310	0.24	179	0.19	131	0.30
8	842	0.02	407	0.00	435	0.10

than in April (50–60 ppb), consistent with either a higher global northern hemisphere summer ozone production or stratospheric intrusions occurrence. High O$_3$ layers (>70 ppb) coinciding with low CO concentrations ($\sim$110 ppb) are encountered on Flights 5, 6 and 8 (Fig. 7), at altitudes above 5 km, and usually at the highest points of the flight (7 km). According to the weather and transport analysis of this campaign (see Section 3) this is due to a fast zonal transport with a footprint spanning North America, North Atlantic and Europe. For instance on Flight 5 an air mass (profiles 5–6 at 6–7 km, Fig. 7d) with high O$_3$ and low CO (respectively 65.0 ± 4.0 ppb and 101.7 ± 5.8 ppb) also exhibits a low ($5 \pm 3\%$) relative humidity. This is consistent with a stratospheric contribution to higher O$_3$ concentrations, although our transport model also suggests a significant contribution to O$_3$ precursors from long-range transport of biomass burning plumes. Enhanced O$_3$ and CO concentrations occur in lower troposphere biomass burning plumes on Flight 5 (Figs. 7b and c; see Section 4.2.2).

On Flights 5–7, below 1.5 km (in the BL), O$_3$ concentrations are systematically lower than 40 ppb. These BL O$_3$ anomalies are not correlated with any CO enhancement (Fig. 9d). Below 3 km, at best, a correlation of $R^2 = 0.08$ is found during Flight 7. This absence of relation discards the role of local pollution in the O$_3$ depletion, via reaction with recently emitted NO. The BL lower O$_3$ concentrations are attributed to deposition on the vegetation and soil on large scales. O$_3$ dry deposition seems to be stronger in September than in April. In the BL, this large, continental-scale deposition is consistent with lower summer values relative to spring despite higher summer photochemical production.

5. A case study for the source attribution of CO and CO$_2$ enhancements in April 2006

5.1. Uplift of elevated CO concentrations from China in April

We investigated the origin of abnormally high CO and CO$_2$ concentrations (mean CO 220 ppb and CO$_2$ 391 ppm) encountered

on 12 April 2006 in the upper parts of Flight 2 and 3, in eastern Siberia (Figs. 6c–f). Note that Flight 1 is not reached by the abnormally high CO and CO$_2$ concentrations. Maximum CO and CO$_2$ values in the FT reached 255 ppb and 392.2 ppm, respectively, on Flight 3 (Fig. 6e at 6 km altitude). This air mass has a distinctly high positive correlation between CO$_2$ and CO ($R^2 = 0.53$ when taking all the 12 profiles of Flights 2–3 above 3.5 km) and there is a finely (500–1000 m) stratified structure. Under 3 km, in contrast, CO and CO$_2$ exhibit near-background concentrations.

5.1.1. Fast transport modelling related to a baroclinic perturbation. Figure 10 shows the uplift event as described by backward transport analysis. At the altitude where they are observed, these elevated CO and CO$_2$ concentrations are unlikely to reflect emissions from Siberian cities. This is confirmed by the 6-d HYSPLIT back-trajectories analysis and by the surface PES footprints calculated with the FLEXPART model (Fig. 10a). HYSPLIT version 4 (Draxler et al., 1997) back-trajectories were run from the position and time where the highest CO concentration was recorded during Flight 2 over Yakutsk. The green circles on each trajectory mark 24 h intervals. Back-trajectories were computed 6 d backwards from three different starting times bracketing the actual sampling time by ± 1 h. In Fig. 10a the FLEXPART model was limited to 10 d of backward transport, with clouds of particles being released at locations where measured CO exceeded 220 ppb. Figure 10a also shows ATSR hot spots.

Figure 10b shows the back-trajectory vertical displacement. Together with Fig. 10a it reveals the following sequence: a flow towards the Pacific was dominant at low altitudes over northeastern China. This air stream was eventually redirected northward by frontal activity near the coast between China and Japan and uplifted from the BL. The uplift happened between 30 and 50 h prior to the sampling and lofted polluted air at 6 km altitude. The airstream finally remained homogeneous and reached Flight 2 in thin polluted layers as shown by our data.

Figures 10c and d shows the measured and simulated CO enhancements during Flights 2 and 3. Retro-transport was extended here to 20 d backward to probe sensitivity to remote influences. The EDGAR 3.2 FT 2000 emissions (Olivier et al., 2005) emission inventory is used. The CO enhancement above background, caused by recent sources, is obtained by convolving the PES with the CO emission map. Therefore, as the backward transport is run only for 20 d, the pertaining CO concentrations are only the enhancements due to contact with emissions in the last 20 d, with a prescribed chemical lifetime. There is no model spin-up with respect to chemical composition and therefore in this case, FLEXPART cannot simulate a background concentration.

The CO enhancement in Flight 2 at 0330 UTC is correctly modelled but underestimated by a factor of 3. The CO peak at 0445 UTC is also underestimated and located 1.5 km too high by the model. Some peaks are underestimated by a factor of 10. The sources of error in this comparison are (1) time or altitude
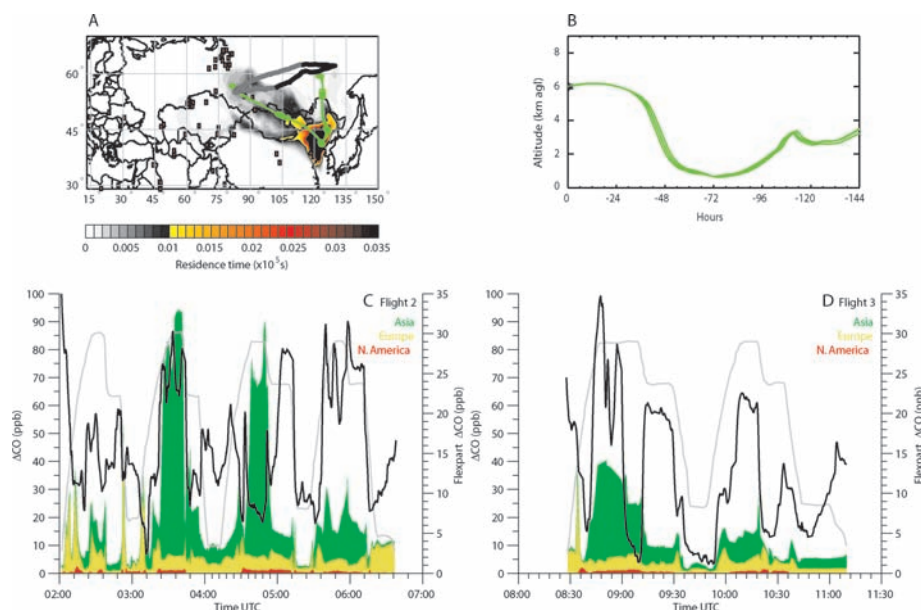
Fig. 10. Flights 2 and 3: Export of polluted boundary layer air with high CO concentrations to Eastern Siberia, 12 April 2006. (a) FLEXPART residence time below 1.5 km for 10 d backward. Model particles are released at aircraft times and positions only when actual measured CO > 220 ppb. As a complement, the light green track represent 4 HYSPLIT backtrajectories run at 1 h interval around aircraft passage at 0600 UTC, at 129°E 62°N and altitude 6 km (matching detection of a CO peak). (b) Vertical movement of the same backtrajectories with 4 releases at 1 h interval. Note the rapid uplift 2–3 d prior to detection. (c) Measured ΔCO (black line) and simulated ΔCO by origin during Flight 2 (Asia in green, Europe in yellow and North America in red, cumulative filled areas, right *Y*-axis scale). Altitude is shown normalized as grey line. (d) same as (c) for Flight 3 (same day).

mismatch (phase error) in the model, (2) under-estimation of CO emissions from Chinese industrial activities and biofuel burning in EDGAR, leading to too low concentrations in Asian out-flow (Petron et al., 2002; Streets et al., 2003; Forster et al., 2004; Akimoto et al., 2006) or (3) additional CO from biomass burning (fires are not included in our simulation). In a multiyear study, Petron et al. (2002) highlighted the need for nearly a doubling of Asian emissions compared to a priori inventory (EDGAR) to keep consistency between atmospheric measurements and emissions. Additionally, FLEXPART simulates poorly local pollution at low altitudes, probably due to non-representation of (1) emissions in Siberia and (2) night-time accumulation of pollutants.

The FLEXPART model predicts high CO enhancements between 5 and 7 km altitude from North East Asian emissions, and a clean lower troposphere, reflecting the observed CO concentrations. Despite phase errors and underestimations the model is able to show that the middle troposphere (5–7 km altitude) has marked CO enhancements compared to the lower troposphere, and that these enhancements originate from transport of Asian pollution. Figure 10a shows that the sensitivity to Asian emissions is particularly marked over North Eastern China.

Spring is the peak season of desert dust storms in northeastern Asia. An extremely high atmospheric dust load was observed in April 2006 over Beijing (Papayannis et al., 2007), corresponding to a large fraction of coarse particles (AOD > 3 at 440 nm). After its passage over industrialized regions of northern China,

this dust-loaded air mass was later sampled during our Flight 2. The high dust load could explain low O_3 concentration of this plume.

5.1.2. Warm conveyor belts role on Asian pollutants redistribution. To our knowledge, no direct observation of fast upward transport of a polluted airstream from northern Asia into the Siberian mid troposphere has been made before. Rapid uplift and subsequent transport of BL air occurs generally in mid-latitude cyclones (Cooper et al., 2001). Warm conveyor belts (WCB) vigorously uplift moist boundary-layer air ahead of cold fronts (Berkowitz et al., 1996; Vaughan et al., 2003). They are most frequent on the eastern coast of continents (Eckhardt et al., 2004), so Siberia is expected to be only a marginal receptor of recently uplifted WCB air masses (Stohl, 2001; his Plate 1). To separate the contributions of uplifted Asian pollution and other sources to the CO enhancements (ΔCO) observed in Flights 2 and 3, the CO enhancements simulated by FLEXPART (Fig. 10c) have been split by continent of origin (results for all flights available at http://zardoz.nilu.no/~andreas/YAK/).

When averaging the modelled enhancement ΔCO time series over the whole flight, European emissions contribute 32.4% to ΔCO, Asia 64.4%, and North America 3.2% only. The modelled contribution of European CO emissions is homogeneously distributed throughout the time series whereas the contribution of Asian emissions is more localized into layers above 3.5 km (Fig. 10c). As a result, below 3.5 km, the European contribution

to the anomaly represents 71%, but conversely the Asian contribution constitutes 71% of the ΔCO above this altitude. As an example, in the layer observed at 0330 UTC in Fig. 10c, CO from Asian sources has a 10-fold higher contribution than CO from European sources.

In their characterization of the mean transport of pollutants across Siberia, Newell and Evans (2000) show that maximum zonal flow is usually prevailing in winter and early spring, which is associated to a European footprint. Ramonet et al. (2002) identified European anthropogenic emissions to be the main contributor to the synoptic variability of CO_2 at an aircraft site located 300 km from Moscow. The April 2006 YAK-AEROSIB campaign data suggests that episodic and rapid transport of northeast Asian emissions can contribute to the mid and high Siberian troposphere composition, in addition to the zonal advection of European emissions. The delivery of pollutants to the Siberian troposphere by WCB airstreams could be underestimated in coarse resolution global Chemistry Transport Models, which do not capture correctly these synoptic events.

5.1.3. Limited chemistry in the plume. The O_3 concentrations in the polluted (CO > 200 ppb) air mass is in the range 55–60 ppb (Figs. 6c–f). It shows no correlation with CO ($R^2 = 0.08$). In addition we found evidence for enhanced (up to 2×10^{-2} cm^{-3}, that is, one order of magnitude above background) concentrations of fine particles (CCN aerosols) in these pollution layers from onboard instruments measuring particles with diameter $d < 200$ nm (Arshinov et al., 2007). Coarse dust particles were not measured during the campaign. High concentration levels of fine aerosol particles, and potentially coarse particles, in the air stream might have led to additional O_3 destruction via heterogeneous reactions (e.g. Bonansoni et al., 2004).

5.1.4. Contributions of biomass burning and fossil fuel combustion. The elevated CO and CO_2 levels are consistent with a mix of urban pollution and biomass burning emissions (wildfires or agricultural fires). Several fires were detected in April 2006 in the footprint of Flight 2 (see ATSR fire counts, red squares, on Figs. 3b, d and 10a). According to FLEXPART simulations Flight 2 sampled CO and CO_2 from fire emissions from northern Mongolia (in the region 50°N and 105–120°E) and northern high latitudes in addition to heavy anthropogenic emissions from northern China. The CO/CO_2 regression slope ($S = 1.17 \times 10^{-2}$) in Flight 2 is consistent with a predominant contribution of anthropogenic emissions; this will be discussed in Section 5.2.

5.2. Interpretation of CO/CO_2 ratio for selected cases

5.2.1. CO as a surrogate tracer for fossil fuel CO_2. We investigated whether CO can be used quantitatively to identify the fossil fuel component of CO_2, given that fossil fuel combustion emits both CO and CO_2 (see also e.g. Gamnitzer et al., 2006; Rivier et al., 2006; Turnbull et al., 2006; Levin and Karstens, 2007). The difficulty in using CO as a proxy of fossil fuel CO_2 is that the CO/CO_2 emission ratio varies spatially and temporally,

Table 3. CO/CO_2 ratio for regional emissions and ΔCO/ΔCO_2 as measured during the YAK-1 campaign. Units are $\times 10^{-2}$ mol mol^{-1} for EDGAR emissions and $\times 10^{-2}$ ppm ppm^{-1} for the measurements. The EDGAR ratio uncertainties are given in the 95% confidence interval

CO/CO_2, EDGAR ($\times 10^{-2}$)		
China (1)		2.13 ± 2.20
Europe (2)		1.08 ± 0.50
ΔCO/ΔCO_2, Our data ($\times 10^{-2}$)		
Flight 2, <3km		0.66
	CO > 200 ppb	CO < 200 ppb
Flight 2, Profiles 7–8	1.25	0.69
Flight 3, Profiles 1–4	1.39	0.52
Flight 2, Profile 6, in high CO plume	1.94	–

Note: (1) Represents average over the region bracketed in latitude by [25N 52N] and in longitude by [80E 135E] and (2) represents average over the region [35N 65N], [10W 55E].

according to the mix of combustion processes (from 1.38×10^2 mol mol^{-1} for western northern hemisphere industrial processes to 6.83×10^2 mol mol^{-1} for world average road transportation, according to the EDGAR inventory). For this study we use the ratio of CO to CO_2 in anthropogenic emissions as given by the EDGAR 3.2 Fast-Track 2000 dataset (Olivier et al., 2005). The average fossil fuel CO/CO_2 emission ratio is 1.08×10^{-2} mol mol^{-1} in Western Europe, compared to 2.13×10^{-2} in China (Table 3, see following section for a discussion on uncertainties). The CO/CO_2 emission ratio of biomass burning is higher than the one of fossil fuel combustion: $10.7 \pm 3.8 \times 10^{-2}$ for extratropical forest fires, $7.9 \pm 3.2 \times 10^{-2}$ for bio-fuel burning, $12.0 \pm 2.5 \times 10^{-2}$ for charcoal burning, and $9.5 \pm 8.8 \times 10^{-2}$ for agricultural residues burning (Andreae and Merlet, 2001).

The distribution of CO/CO_2 ratios in the global atmosphere results from (1) atmospheric transport which mixes the ratios of different emission sources, (2) secondary CO production from biogenic volatile organic compounds (BVOC) and atmospheric sinks of CO from OH oxidation which change CO but not CO_2 and (3) terrestrial and oceanic surface CO_2 fluxes which change CO_2 but not CO.

In winter-times, the effect of processes (2) and (3) is limited. Note the significantly higher CO–CO_2 correlation for Flight 4 which was sampled only in the morning, unlike the other April flights (see Table 2). Positive correlations between CO and CO_2 are frequently found at northern hemisphere stations (Potosnak et al., 1999; Suntharalingam et al., 2004; Gamnitzer et al., 2006; Palmer et al., 2006; Rivier et al., 2006). Potosnak et al. (1999) observed that using CO as a predictor for CO_2 was more effective in winter. In a northern hemisphere modelling study, Rivier

et al. (2006) predicted ubiquitous wintertime correlations between CO and fossil CO_2. They also showed that the modelled scatter between CO and fossil CO_2 was caused by advection of air masses with different CO/CO_2 emission ratios (see their Fig. 6).

5.2.2. CO/CO_2 ratios during Flights 2 and 3 and source attribution. One can decompose the CO_2 and CO concentration as the sum of the background value (determined as in Section 4) and an anomaly called ΔCO_2 and ΔCO, respectively. We regressed the observed value of ΔCO as a function of ΔCO_2 for all flights (see Fig. 9 and Table 2 for correlation coefficients). In the April campaign, there is a significant positive correlation between ΔCO and ΔCO_2, with a clear distinction between data above and below 3.5 km (for Flight 2 $R^2 = 0.58$ below 3.5 km and $R^2 = 0.55$ above). Above 3.5 km in April Flights 2 and 3 (Figs. 9b and c), the regression slope is clearly higher than for Flight 1 and 4 (Figs. 9a and d), and also higher than below 3.5 km for the same flights. The $\Delta CO/\Delta CO_2$ linear regression slopes are 6.8 and 11.3 ppb ppm^{-1}, respectively below and above 3.5 km. This high, positive CO-CO_2 correlation coefficient suggests that the contribution of natural CO_2 fluxes and photo-chemical CO sinks to this flight is small. This is further confirmed by combining the CO_2 Net Ecosystem Exchange (NEE) fluxes calculated by the ORCHIDEE process-based ecosystem model (Krinner et al., 2005) at $0.4 \times 0.4°$ in April 2006 with the FLEXPART footprints. For the entire April 2006 YAK-AEROSIB campaign, we found that the contribution of NEE is negligible relative to anthropogenic fluxes: –0.5% for Europe (i.e. small biospheric uptake) and +1.1% for Asia relative to fossil fuel emissions. Thus, neglecting the impact of natural CO_2 sources to the vertical variability in the April profiles, ΔCO_2 can be expressed from ΔCO by:

$$\Delta CO_2(obs) = \Delta CO(obs) \times S^{-1} + constant, \quad (1)$$

where the constant term represents the background CO_2 component, assumed to be vertically uniform in each profile. For the situation of Flights 2 and 3 we assumed that, in presence of fast horizontal transport of remote emissions and comparatively lower vertical mixing, the value of S reflects the ratio of fossil fuel emissions, weighted by the emitted flux over each grid point (see Gamnitzer et al., 2006). Using the EDGAR 3.2 Fast-Track 2000 fossil fuel CO and CO_2 emission maps, the emission ratio are $S = 2.13 \times 10^{-2}$ mol mol^{-1} for China, $S = 1.08 \times 10^{-2}$ mol mol^{-1} for Europe. Thus, the *ratio* of Chinese emissions CO/CO_2 ratio to the European CO/CO_2 is 1.97. In the YAK-AEROSIB data, the ratio of Asian (above 3.5 km) to European (below 3.5 km) CO/CO_2 ratios in the Eastern part of the campaign is 1.8.

5.2.3. Analysis of errors. The ratio of European to Asian $\Delta CO/\Delta CO_2$ in the YAK measurements is consistent with that of emission inventories. However, the values of the $\Delta CO/\Delta CO_2$ slope S determined from the YAK measurements are half the values given by inventories (Table 3). Significant error sources in the inventories propagate to the slopes. We computed a 95% confidence uncertainty for Asian and European emission CO/CO_2 slopes using a Monte Carlo analysis. We assume a weak correlation ($R^2 = 0.1$ as suggested by Palmer et al., 2006) between CO and CO_2 emission uncertainties, due to the presence of correlated error sources in the underlying emission factors and activities. A rough estimate of the error for CO and CO_2 Asian emissions is 50 and 20%, respectively (Streets et al., 2003), and for European emissions of 30 and 10%, respectively. The Monte Carlo simulation gives emission CO/CO_2 slopes $S = 2.1 \pm 2.2 \times 10^{-2}$ mol mol^{-1} for Asian and $1.1 \pm 0.50 \times 10^{-2}$ mol mol^{-1} for Europe.

Into the polluted air masses of Flights 2–3 where CO > 200 ppb, we determined $S = 12.5$ ppb ppm^{-1} for Flight 2 (profiles 7–8, and $S = 13.9$ ppb ppm^{-1} for Flight 3 (profiles 1–4). Taking only data inside the plume of profiles 6–7 of Flight 2 at 5 km altitude (Fig. 6c) we obtain $S = 19.4$ ppb ppm^{-1}. All these values are given in Table 3. Therefore, the more we restrict the CO data selection towards elevated values representative of polluted air masses, the better agreement is found for S between atmospheric data and inventories, and the more accurate our discrimination of Asian vs. European emissions. This suggests that the $\Delta CO/\Delta CO_2$ signal is significantly diluted (1) as a methodological flaw when averaging over distinct air masses and (2) physically when mixing with the surrounding air takes place. This dilution can result in lower $\Delta CO/\Delta CO_2$ ratio because the enhancement relative to background is higher for CO than for CO_2.

The precision of our method, based on deviation from background concentration, is affected by other factors, such as the absence of simple (e.g. marine) background. However the *ratio* between S in the lower and S in the upper part of the profiles is consistent with the retro-transport analysis of a dominant Chinese pollution influence above 3.5 km, and of a dominant European origin below that altitude. Due to limited mixing, the conservation of CO/CO_2 ratios in the YAK easternmost flights was similar to that of the TRACE-P flights with high ($R^2 > 0.7$) CO–CO_2 correlations at all altitudes analysed by Suntharalingam et al. (2004), which allowed Palmer et al. (2006) to use CO–CO_2 error covariance for better separating Asian fossil from biogenic CO_2 fluxes. Under most common conditions, CO/CO_2 ratio is not a conservative tracer. The uplift situation of April 2006 was specifically favourable to preserve high CO/CO_2 correlations over long distances because: (1) there was no biotic CO_2 sinks in Siberia at this time of the year and (2) the air mass was sampled after uplift, before being homogenized and mixed by transport, and thus contained a well defined CO/CO_2 signature.

6. Conclusion

The set-up and preliminary results of two YAK-AEROSIB aircraft campaigns across Siberia in April and September 2006

have been presented. Each campaign comprises four flights and a total of 26 vertical profiles spaced by 200 km between 0 and 7 km. We report here on the in situ measurement of CO_2, CO and O_3. The April 2006 campaign was characterized by a slow zonal flow, and the influence of Siberian cities and remote Asian emissions in the vertical profiles. The September 2006 campaign was dominated by meandering zonal flow, variable synoptic conditions and a descent of arctic air in the boundary layer (BL). Both CO_2 and CO values were very high in April 2006 (respectively 385–390 ppm and 160–200 ppb) due to both near-ground accumulation of Siberian cities emissions, and long-range transport in the middle troposphere. The lowest CO_2 concentration values were observed in the BL during September, which support the view of a strong biospheric CO_2 sink in Siberia at that time of the year. The next step will be to analyse the CO_2 data within a regional inverse model (Lauvaux et al., 2007) in order to exploit quantitatively the information contained in the CO_2 gradients.

In the free troposphere (FT), the O_3 concentrations were much more homogeneous than those of CO_2 and CO across the whole aircraft transect. In April O_3 values smoothly increased with altitude u to the flight ceiling. In September a 20 ppb gradient of O_3 was observed between the FT and the ozone-depleted BL. This gradient is likely due to O_3 deposition over the forests and to a stronger late summer turbulent mixing. The relationships between O_3 and CO (indicator of O_3 precursors) analysed from the April 2006 campaign have not shown important active photochemistry from regional fresh emissions. Relatively high O_3 levels (50–65 ppb) in the FT (both in April and September) reflect the global northern hemisphere O_3 enhancement.

The mid troposphere in the eastern part of the April campaign exhibited very high CO and CO_2 values. Analysis of this air mass using back-trajectories and a Lagrangian transport model revealed the effect of a sequence of baroclinic perturbations followed by stagnant conditions in the middle troposphere. This led to the fast injection and persistence for several days over Siberia of thin layers of polluted air originating from northeastern Asian sources. The export of Asian pollution to the East through the Pacific Ocean at mid-latitudes is partially driven by cold front uplift (see e.g. Mari et al., 2004). This export pathway has been extensively documented (see e.g. Jacob et al., 2003; Suntharalingam et al., 2004), contrarily to the northward transport of Asian emissions towards Siberia. Our observations has shown that the advection of BL air exposed to Asian emissions and uplifted Warm Conveyor Belt contributed significantly to the CO_2 and CO enhancement of the upper Siberian troposphere during April 2006. This case of export pattern deserves further investigation, especially using chemistry—transport modelling.

CO has been suggested as a tool for separating the fossil CO_2 component in the observed total CO_2 signals. In our study we have been able to use CO/CO_2 ratio in the free troposphere, even far from the emission regions, as a quantity representative of surface emissions characteristics. Therefore, under specific conditions, atmospheric CO/CO_2 ratios could be used for separating source regions with contrasted emission ratios, like Asia and Europe. In September, with more active chemistry and production of CO from VOCs, this property was no longer valid.

7. Acknowledgments

References

Akimoto, H. 2003. Global air quality and pollution. *Science* **302**(5651), 1716–1719.

Akimoto, H., Ohara, T., Kurokawa, J. and Horii, N. 2006. Verification of energy consumption in China during 1996–2003 by using satellite observational data. *Atmos. Environ.* **40**, 7663–7667.

Andreae, M. O. and Merlet, P. 2001. Emission of trace gases and aerosols from biomass burning. *Global Biogeochem. Cycles.* **15**(4), 955–966.

Arshinov, M. Yu., Belan, B. D., Nedelec, Ph., Paris, J.-D. and Machida, T. 2007. Spatial distribution of nanoparticles in the free troposphere over Siberia. In: *Nucleation and Atmospheric Physics, 17th International Conference on Nucleation and Atmospheric Aerosols, Galway, Ireland, 2007* (eds C. D. O'Dowd and P. E. Wagner) Springer, New York, 819–823.

Bartalev, S. A., Belward, A. S., Erchov, D. V. and Isaev, A. S. 2003. A new SPOT4-VEGETATION derived land cover map of Northern Eurasia. *Int. J. Remote Sens.* **24**(9), 1977–1982.

Beekmann, M., Ancellet, G. and Mégie, G. 1994. Climatology of tropospheric ozone in Southern Europe and its relation to potential vorticity. *J. Geophys. Res.* **99**(D6), 12841–12853.

Bergamaschi, P., Brenninkmeijer, C. A. M., Hahn, M., Rockmann, T., Scharffe, D. H. and co-authors. 1998. Isotope analysis based source identification for atmospheric CH4 and CO sampled across Russia using the Trans-Siberian railroad. *J. Geophys. Res.* **103**(D7), 8227–8235.

Berkowitz, C. M., Daum, P. H., Spicer, C. W. and Busness, K. M. 1996. Synoptic patterns associated with the flux of excess ozone to the western North Atlantic. *J. Geophys. Res.* **101**(D22), 28923–28933.

Bey, I., Jacob, D. J., Logan, J. A. and Yantosca, R. M. 2001. Asian chemical outflow to the Pacific in spring: origins, pathways, and budgets. *J. Geophys. Res.* **106**(D19), 23097–23113.

Bonasoni, P., Cristofanelli, P., Calzolari, F., Bonafè, U., Evangelisti, F. and co-authors. 2004. Aerosol-ozone correlations during dust transport episodes. *Atmos. Chem. Phys.* **4**, 1201–1215.

Chan, D., Yuen, C. W., Higuchi, K., Shashkov, A., Liu, J. and co-authors. 2004. On the CO_2 exchange between the atmosphere and the biosphere: the role of synoptic and mesoscale processes. *Tellus* **56B**, 194–212.

Cooper, O. R., Moody, J. L., Parrish, D. D., Trainer, M., Ryerson, T. B. and co-authors. 2001. Trace gas signatures of the airstreams within North Atlantic cyclones: case studies from the North Atlantic Regional Experiment (NARE '97) aircraft intensive. *J. Geophys. Res.* **106**(D6), 5437–5456.

Crutzen, P. J., Elansky, N. F., Hahn, M., Golitsyn, G. S., Brenninkmeijer, C. A. M. and co-authors. 1998. Trace gas measurements between Moscow and Vladivostok using the Trans-Siberian Railroad. *J. Atmos. Chem.* **29**(2), 179–194.

Draxler, R. R. and Hess, G. D. 1997. *Description of the Hysplit 4 Modeling System*. NOAA Tech Memo ERL ARL-224, December, 24p.

Eckhardt, S., Stohl, A., Wernli, H., James, P., Forster, C. and co-authors. 2004. A 15-year climatology of warm conveyor belts. *J. Clim.* **17**(1), 218–237.

Forster, C., Cooper, O., Stohl, A., Eckhardt, S., James, P. and co-authors. 2004. Lagrangian transport model forecasts and a transport climatology for the Intercontinental Transport and Chemical Transformation 2002 (ITCT 2k2) measurement campaign. *J. Geophys. Res.* **109**, D07S92, doi:10.1029/2003JD003589.

Gamnitzer, U., Karstens, U., Kromer, B., Neubert, R. E. M., Meijer, H. A. J. and co-authors. 2006. Carbon monoxide: a quantitative tracer for fossil fuel CO_2? *J. Geophys. Res.* **111**(D22), D22302, doi:10.1029/2005JD006966.

Gerbig, C., Lin, J. C., Wofsy, S. C., Daube, B. C., Andrews, A. E. and co-authors. 2003. Toward constraining regional-scale fluxes of CO_2 with atmospheric observations over a continent: 1. Observed spatial variability from airborne platforms. *J. Geophys. Res.* **108**(D24), 4757, doi:10.1029/2003JD003770.

Gurney, K. R., Law, R. M., Denning, A. S., Rayner, P. J., Baker, D. and co-authors. 2002. Towards robust regional estimates of CO_2 sources and sinks using atmospheric transport models. *Nature* **415**(6872), 626–630.

Hiyama, T., M. A.S., Suzuki, R., Asanuma, J., Mezrin, M. Y., Bezrukova, N. A. and co-authors. 2003. Aircraft observations of the atmospheric boundary layer over a heterogeneous surface in eastern Siberia. *Hydrol. Process.* **17**(14), 2885–2911.

Jacob, D. J., Fan, S. M., Wofsy, S. C., Spiro, P. A., Bakwin, P. S. and co-authors. 1992. Deposition of Ozone to Tundra. *J. Geophys. Res.* **97**(D15), 16473–16479.

Krinner, G., Viovy, N., de Noblet-Ducoudre, N., Ogee, J., Polcher, J. and co-authors. 2005. A dynamic global vegetation model for studies of the coupled atmosphere-biosphere system. *Global Biogeochem. Cycles* **19**, GB1015, doi:10.1029/2003GB00219.

Lauvaux, T., Uliasz, M., Sarrat, C., Chevallier, F., Bousquet, P. and co-authors. 2007. Mesoscale inversion: first results from the CERES campaign with synthetic data. *Atmos. Chem. Phys. Discuss.* **7**, 10439–10465.

Levin, I. and Karstens, U. 2007. Inferring high-resolution fossil fuel CO_2 records at continental sites from combined (CO_2)-C-14 and CO observations. *Tellus* **59B**, 245–250.

Levin, I., Ciais, P., Langenfelds, R., Schmidt, M., Ramonet, M. and co-authors. 2002. Three years of trace gas observations over the EuroSiberian domain derived from aircraft sampling—a concerted action. *Tellus* **54B**, 696–712.

Lin, J. C., Gerbig, C., Wofsy, S. C., Andrews, A. E., Daube, B. C. and co-authors. 2003. A near-field tool for simulating the upstream influence of atmospheric observations: the Stochastic Time-Inverted Lagrangian Transport (STILT) model. *J. Geophys. Res.* **108**(D16), doi:10.1029/2002JD003161.

Lloyd, J., Langenfelds, R. L., Francey, R. J., Gloor, M., Tchebakova, N. M. and co-authors. 2002. A trace-gas climatology above Zotino, central Siberia. *Tellus* **54B**, 749–767.

Machida, T., Nakazawa, T., Ishidoya, S., Maksyutov, S., Tohjima, Y. and co-authors. 2001. Temporal and spatial variations of atmospheric CO_2 mixing ratio over Siberia. *Proceedings of the 6th International Carbon Dioxide Conference*, 1–5 October 2001, Sendai, Japan . 15–18.

Maksyutov, S., Machida, T., Shimoyama, K., Carouge, C., Peregon, A. and co-authors. 2006. Top-down approach to West Siberian regional carbon budget: combination of the CO_2 observations and inverse modelling. *Eos Trans. AGU.* **87**(52), Fall Meet. Suppl., Abstract GC21B-02

Mari, C., Evans, M. J., Palmer, P. I., Jacob, D. J. and Sachse, G. W. 2004. Export of Asian pollution during two cold front episodes of the TRACE-P experiment. *J. Geophys. Res.* **109**(D15), doi:10.1029/2003JD004307.

Nakazawa, T., Sugawara, S., Inoue, G., Machida, T., Makshyutov, S. and co-authors. 1997. Aircraft measurements of the concentrations of CO_2, CH4, N2O, and CO and the carbon and oxygen isotopic ratios of CO_2 in the troposphere over Russia. *J. Geophys. Res.* **102**(D3), 3843–3859.

Nédélec, P., Cammas, J. P., Thouret, V., Athier, G., Cousin, J. M. and co-authors. 2003. An improved infrared carbon monoxide analyser for routine measurements aboard commercial Airbus aircraft: technical validation and first scientific results of the MOZAIC III programme. *Atmos. Chem. Phys.* **3**, 1551–1564.

Nédélec, P., Thouret, V., Brioude, J., Sauvage, B., Cammas, J. P. and co-authors. 2005. Extreme CO concentrations in the upper troposphere over northeast Asia in June 2003 from the in situ MOZAIC aircraft data. *Geophys. Res. Lett.* **32**(14), L14807, doi:10.1029/2003JD004307.

Newell, R. E. and Evans, M. J. 2000. Seasonal changes in pollutant transport to the North Pacific: the relative importance of Asian and European sources. *Geophys. Res. Lett.* **27**(16), 2509–2512.

Newell, R. E., Thouret, V., Cho, J. Y. N., Stoller, P., Marenco, A. and co-authors. 1999. Ubiquity of quasi-horizontal layers in the troposphere. *Nature.* **398**(6725), 316–319.

Nicholls, M. E., Denning, A. S., Prihodko, L., Vidale, P.-L., Baker, I. and co-authors. 2004. A multiple-scale simulation of variations in atmospheric carbon dioxide using a coupled biosphere-atmospheric model. *J. Geophys. Res.* **109**, D18117, doi:10.1029/2003JD004482.

Oberlander, E. A., Brenninkmeijer, C. A. M., Crutzen, P. J., Elansky, N. F., Golitsyn, G. S. and co-authors. 2002. Trace gas measurements along the Trans-Siberian railroad: the TROICA 5 expedition. *J. Geophys. Res.* **107**(D14), 4206, doi:10.1029/2001JD000953.

Olivier, J. G. J., Van Aardenne, J. A., Dentener, F., Ganzeveld, L. and Peters, J. A. H. W. 2005. Recent trends in global greenhouse gas

emissions: regional trends and spatial distribution of key sources. in *Non-CO₂ Greenhouse Gases (NCGG-4)* (ed. A.v. Amstel). Millpress, Rotterdam, 325–330.

Palmer, P. I., Suntharalingam, P., Jones, D. B. A., Jacob, D. J., Streets, D. G. and co-authors. 2006. Using CO_2:CO correlations to improve inverse analyses of carbon fluxes. *J. Geophys. Res.* **111**(D12), doi:10.1029/2005JD006697.

Papayannis, A., Zhang, H. Q., Amiridis, V., Ju, H. B., Chourdakis, G. and co-authors. 2007. Extraordinary dust event over Beijing, China, during April 2006: Lidar, Sun photometric, satellite observations and model validation. *Geophys. Res. Lett.* **34**(7), L07806, doi:10.1029/2006GL029125.

Petron, G., Granier, C., Khattatov, B., Lamarque, J. F., Yudin, V. and co-authors. 2002. Inverse modeling of carbon monoxide surface emissions using Climate Monitoring and Diagnostics Laboratory network observations. *J. Geophys. Res.* **107**(D24), 4761, doi:10.1029/2001JD001305.

Pochanart, P., Akimoto, H., Kajii, Y., Potemkin, V. M. and Khodzher, T. V. 2003. Regional background ozone and carbon monoxide variations in remote Siberia/East Asia. *J. Geophys. Res.* **108**(D1), doi:10.1029/2001JD001412.

Potosnak, M. J., Wofsy, S. C., Denning, A. S., Conway, T. J., Munger, J. W. and co-authors. 1999. Influence of biotic exchange and combustion sources on atmospheric CO_2 concentrations in New England from observations at a forest flux tower. *J. Geophys. Res.* **104**(D8), 9561–9569.

Ramonet, M., Ciais, P., Nepomniachii, I., Sidorov, K., Neubert, R. E. M. and co-authors. 2002. Three years of aircraft-based trace gas measurements over the Fyodorovskoye southern taiga forest, 300 km northwest of Moscow. *Tellus* **54B**, 713–734.

Rivier, L., Ciais, P., Hauglustaine, D. A., Bakwin, P., Bousquet, P. and co-authors. 2006. Evaluation of SF6, C2Cl4, and CO to approximate fossil fuel CO_2 in the Northern Hemisphere using a chemistry transport model. *J. Geophys. Res.* **111**(D16), doi:10.1029/2005JD006725.

Sarrat, C., Noilhan, J., Lacarrere, P., Donier, S., Lac, C. and co-authors. 2007. Atmospheric CO_2 modeling at the regional scale : application to the CarboEurope Regional Experiment. *J. Geophys. Res.* **112** (D12).

Seibert, P. and Frank, A. 2004. Source-receptor matrix calculation with a Lagrangian particle dispersion model in backward mode. *Atmos. Chem. Phys.* **4**, 51–63.

Stephens, B. B., Gurney, K. R., Tans, P. P., Sweeney, C., Peters, W. and co-authors. 2007. Weak northern and strong tropical land carbon uptake from vertical profiles of atmospheric CO_2. *Science.* **316**(5832), 1732–1735.

Stohl, A. 2001. A 1-year Lagrangian "climatology" of airstreams in the Northern Hemisphere troposphere and lowermost stratosphere. *J. Geophys. Res.* **106**(D7), 7263–7280.

Stohl, A., Forster, C., Frank, A., Seibert, P. and Wotawa, G. 2005. Technical note: the Lagrangian particle dispersion model FLEXPART version 6.2. *Atmos. Chem. Phys.* **5**, 2461–2474.

Stohl, A., Berg, T., Burkhart, J. F., A. M. Fjaeraa, C. and co-authors. 2007a. Arctic smoke—record high air pollution levels in the European Arctic due to agricultural fires in Eastern Europe in spring 2006. *Atmos. Chem. Phys.* **7**, 511–534.

Stohl, A., Forster, C., Huntrieser, H., Mannstein, H., McMillan, W. W. and co-authors. 2007b. Aircraft measurements over Europe of

an air pollution plume from Southeast Asia—aerosol and chemical characterization. *Atmos. Chem. Phys.* **7**, 913–937.

Streets, D. G., Bond, T. C., Carmichael, G. R., Fernandes, S. D., Fu, Q. and co-authors. 2003. An inventory of gaseous and primary aerosol emissions in Asia in the year 2000. *J. Geophys. Res.* **108**(D21), 8809, doi:10.1029/2002JD003093.

Suntharalingam, P., Jacob, D. J., Palmer, P. I., Logan, J. A., Yantosca, R. M. and co-authors. 2004. Improved quantification of Chinese carbon fluxes using CO_2/CO correlations in Asian outflow. *J. Geophys. Res.* **109**(D18), doi:10.1029/2003JD004362.

Turnbull, J. C., Miller, J. B., Lehman, S. J., Tans, P. P., Sparks, R. J. and co-authors. 2006. Comparison of $^{14}CO_2$, CO, and SF_6 as tracers for recently added fossil fuel CO_2 in the atmosphere and implications for biological CO_2 exchange. *Geophys. Res. Lett.* **33**, L01817, doi:10.1029/2005GL024213.

Van Der Molen, M. K. and Dolman, A. J. 2007. Regional carbon fluxes and the effect of topography on the variability of atmospheric CO_2. *J. Geophys. Res.* **112**, D01104, doi:10.1029/2006JD007649.

Vaughan, G., Garland, W. E., Dewey, D. J. and Gerbig, C. 2003. Aircraft measurements of a warm conveyor belt—a case study. *J. Atmos. Chem.* **46**(2), 117–129.

Wang, J. W., Denning, A. S., Lu, L. X., Baker, I. T., Corbin, K. D. and co-authors. 2007. Observations and simulations of synoptic, regional, and local variations in atmospheric CO_2. *J. Geophys. Res.* **112**(D4), doi:10.1029/2006JD007410.

Wild, O., Pochanart, P. and Akimoto, H. 2004. Trans-Eurasian transport of ozone and its precursors. *J. Geophys. Res.* **109**(D11), doi:10.1029/2003JD004501.

Zuev, V. E., Belan, B. D., Kabanov, D. M., Kovalevskii, V. K., Luk'ianov, and co-authors. 1992. The Optik-E AN-30 laboratory-airplane for ecological studies. *Optika Atmosfery i Okeana.* **5**(10), 1012–1021.

Supplementary material

The following supplementary material is available for this article:

Concentration time series

Figure S1. Trace gases concentrations time series for altitude (grey line), O_3 (blue line), CO (red line) and CO_2 (black line) as a function of time and latitude for (a) Flight 1; (b) Flight 2; (c) Flight 3 and (d) Flight 4.

Figure S2. Same as figure S1 but for (a) Flight 5; (b) Flight 6; (c) Flight 7 and (d) Flight 8.

This material is available as part of the online article from: http://www.blackwell-synergy.com/doi/10.1111/j.1600-0889.2008.00369.x

Please note: Blackwell Publishing is not responsible for the content or functionality of any supplementary materials supplied by the authors. Any queries (other than missing material) should be directed to the corresponding author for the article. If authors supply links to their own web sites, the Publisher is not responsible for the material on these sites.